Numerical Simulation of NbTi Superconducting Joint With Cold-Pressing Welding Technology

Feng Zhou, Junsheng Cheng, Jianhua Liu, Yinming Dai, Qiuliang Wang, *Senior Member, IEEE*, Namin Xiao, and Luguang Yan

***Abstract*—The cold-pressing welding methods are employed to fabricate joints between NbTi multifilamentary conductors, and a series of joints are made at different press amounts for nuclear magnetic resonance magnet applications. The Abaqus–Explicit method was used to do a quasi-static analysis of the cold-pressing welding process. In the simulation, we consider the contact area and equivalent plastic strain to determine the resistance of the superconducting joints qualitatively. The simulation shows that a press amount of 61%–65.5% should be the optimum range, in which the lowest joint resistance can be obtained. Resistances of these joints are also tested using the current decay method to verify the simulation.**

***Index Terms*—Abaqus–Explicit methods, cold-pressing welding, NbTi superconducting joint, resistance.**

I. Introduction

NbTi joints are inevitable in the superconducting magnet for nuclear magnetic resonance (NMR) applications due to the limitation of wire length. They are always used to connect two adjacent coils. The persistent current of an NMR magnet is very important, which is dependent upon the resistive losses within the coil circuit [1]. The total resistance in the magnet system comes from superconducting wire resistance and joint resistance [2], [3]. Because the wire resistance can be decreased by increasing the current margin during design, the joints between coils and switches must be carefully fabricated to achieve high magnetic field stability in the NMR system [4].

The joints between NbTi multifilamentary conductors can be fabricated by many methods such as solder welding [5], cold-pressing welding [6], [7] and dip welding, diffusion bonding [8], electromagnetic forming [9], and solder matrix replacement. Among these methods, the cold-pressing welding method is well suited to fabricate NbTi superconducting joints because of its reliability.

In this paper, we used the software Abaqus–Explicit method to simulate a quasi-static analysis of the cold-pressing welding process for NbTi superconducting joints. In the simulation, we mainly considered two factors, i.e., contact area and equivalent plastic strain, to determine the resistance of NbTi joint qualitatively. Resistance testing results were also discussed to verify the conclusion to obtain from the simulation. The purpose of this paper is to find the optimum press amount in the NbTi superconducting joint cold-pressing welding process.

Manuscript received April 25, 2013; revised June 19, 2013 and August 4, 2013; accepted August 5, 2013. Date of current version October 7, 2013. This work was supported in part by the National Natural Science Foundation of China under Grant 50925726 and Grant 10755001 and in part by the Instrument Program of the Ministry of Science and Technology of China. *(Corresponding author: Q. Wang.)*

F. Zhou, J. Cheng, J. Liu, Y. Dai, Q. Wang, and L. Yan are with the Institute of Electrical Engineering, Chinese Academy of Sciences, Beijing 100190, China (e-mail: zhoufeng@mail.iee.ac.cn; qiuliang@mail.iee.ac.cn).

N. Xiao is with the Institute of Metal Research, Chinese Academy of Sciences, Shenyang 110016, China.

Color versions of one or more of the figures in this paper are available online at http://ieeexplore.ieee.org.

Digital Object Identifier 10.1109/TASC.2013.2277779

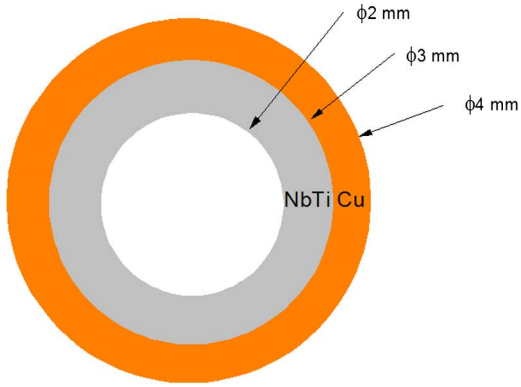

Fig. 1. Schematic cross section of the NbTi/Cu tube.

II. Fabrication of Joints

The NbTi/Cu wire used to fabricate the joints is F54 supplied by Oxford Instruments, which has a bare diameter of 0.4 mm and a Cu/non-Cu ratio of 1.35. The NbTi/Cu tube has a length of 3 cm, an external diameter of 4 mm, and an internal diameter of 2 mm; the configuration of the cross section of the NbTi/Cu tube is shown in Fig. 1. The cold-pressing welding process includes six steps.

1) Remove the insulation layer on the wire by abrasive paper.
2) Remove the stabilizer on the wire by nitric acid until the filaments appear.
3) Clean the filaments by pure water and ethanol.
4) Dry the filaments in open air.
5) Install the filaments in a NbTi/Cu tube.
6) Press the NbTi/Cu tube in open air.

The six NbTi superconducting joints are fabricated with different press amounts. The press amount is defined as

$$p = \frac{\Delta d}{D} \times 100\% \tag{1}$$

where Δd is the press displacement, and D is the external diameter of the NbTi/Cu tube. The press amounts used in this

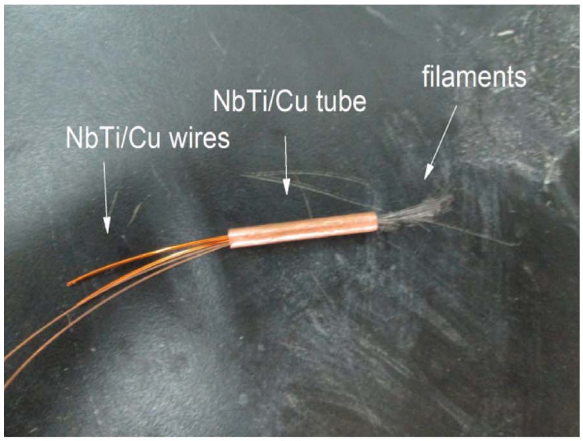

(a)

(b)

Fig. 2. NbTi joint samples. (a) Before press operation. (b) After press operation.

simulation are 49.5%, 54%, 61%, 65.5%, 69.5%, and 70.5%. The samples before and after the press operation are shown in Fig. 2.

III. Simulation

A. Analytical Model

A 3-D finite-element model of the NbTi cold-pressing welding joint was constructed using Abaqus–Explicit. Fig. 3 shows the parameters of the analytical model. To simplify the model, the Cu layer was ignored, and the external diameter of the tube model turns 3 mm. Since NbTi is much harder than Cu, this ignorance will not influence the result seriously. The distribution of filaments is shown in Fig. 3(b). A fully fixed boundary condition was applied on the die, and a displacement boundary condition was applied on the punch. Contact exists between the tube and filaments, as well as among filaments. A general contact was applied to model the complex contact behavior in the process. A Coulomb friction model was used here. We did a NbTi friction experiment to get the friction coefficient equal to 0.72. In addition, 8-noded solid elements (C3D8R) were used for the simulation with nine element layers through the tube thickness and 20 element layers through the tube length.

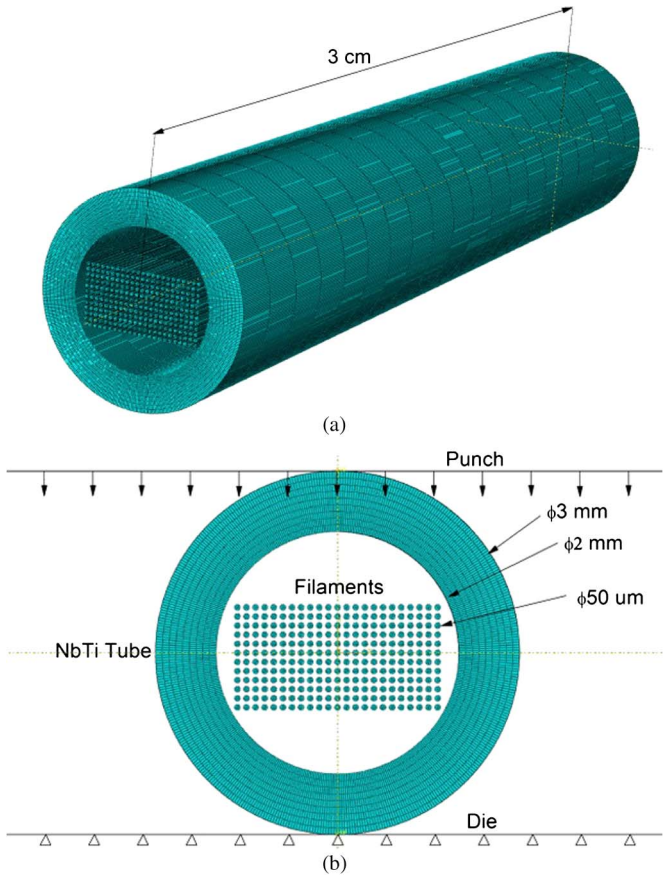

Fig. 3. Parameters of the analytical model. (a) Three-dimensional view. (b) Cross section.

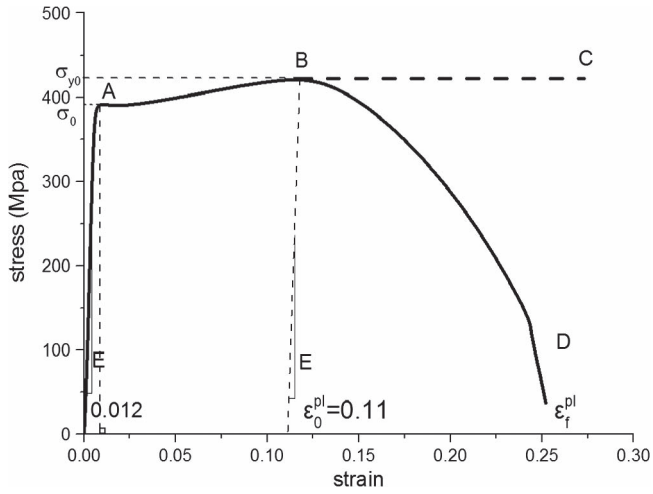

Fig. 4. Stress–strain response curve of the NbTi superconductor.

The input to the model consists of NbTi elastic properties and plastic properties. An elastic-plastic tensile experiment of NbTi was carried out. The result of true stress and logarithmic strain is shown in Fig. 4. From Fig. 4, we get: (a) Elastic modulus is 60.5 GPa; (b) NbTi yields at $\varepsilon = 1.2\%$; and (c) NbTi begins to damage at equivalent plastic strain $\varepsilon_0^{\mathrm{pl}} = 11\%$. Since the stress–strain relationship no longer represents the material's behavior accurately when material necking occurs, an ideal plastic pattern (see BC in Fig. 2) is applied in place of the softening branch (see BD in Fig. 4) [10]. Poisson's ratio, i.e., 0.33, is cited

TABLE I
MAXIMUM KE, CORRESPONDING IE, AND RATIO KE/IE OF THE SIX MODELS

Model	Max KE (J)	Corresponding IE (J)	$\frac{KE}{IE}$
49.5%	0.311	10.316	3.01%
54%	0.378	12.429	3.04%
61%	0.517	14.457	3.58%
65.5%	0.615	15.196	4.05%
69.5%	0.701	15.697	4.47%
70.5%	0.726	16.726	4.34%

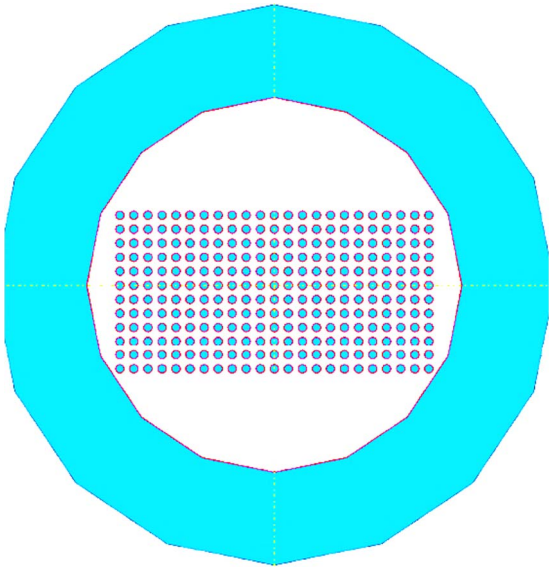

Fig. 5. Definition of contact area (the red region).

from [11]. The density of NbTi, 6027 kg/m^3, can be calculated from the proportion of components Nb 47 wt.% Ti.

B. Load

A displacement boundary condition was applied on the punch to press the tube in the model. It is not necessary to define the analysis time as the actual time since this will make the calculation time too long. We did a quasi-static analysis and defined the analysis time as 0.25 ms to speed up the simulation process. Therefore, the punching speed is ~15 m/s in the model. The press displacement of punch is applied in a smooth step. Table I shows the maximum kinetic energy (KE) and the corresponding internal energy (IE) in the press process of six models. From the ratio KE/IE, we can see that six ratios are all less than 10% (typical threshold) [10]. Hence, according to the energy balance principle, the influence of inertia can be ignored [10], and the analysis time of 0.25 ms is appropriate.

C. Simulation Results and Discussions

Six models with different press amounts with 49.5%, 54%, 61%, 65.5%, 69.5%, and 70.5% were simulated. We mainly consider filaments' contact area and equivalent plastic strain to determine the joint's resistance qualitatively. Since increasing contact is in favor of decreasing joint resistance but increasing strain damage is against that, the lowest joint resistance must be obtained when contact is good and strain damage is small at the same time. However, as the press amount increases, contact area and strain damage will both increase. Therefore, there must be an equilibrium point.

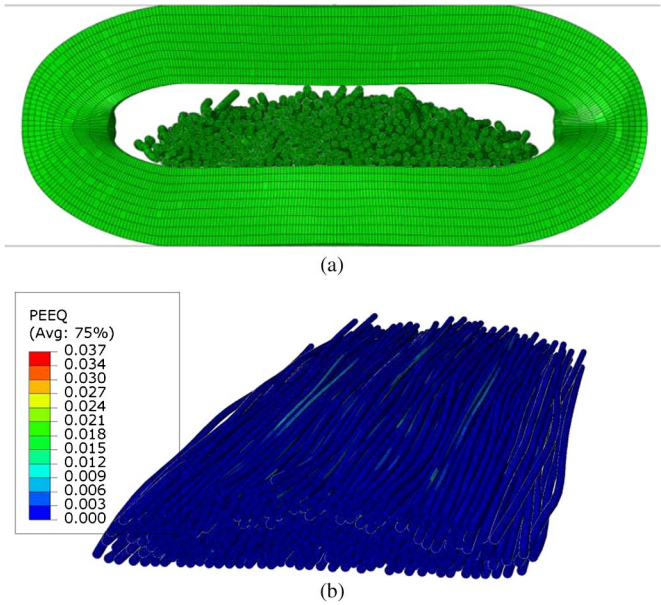

Fig. 6. After press operation. (a) Model cross section. (b) Filaments' equivalent plastic strain distribution for the case with press amount of 49.5%.

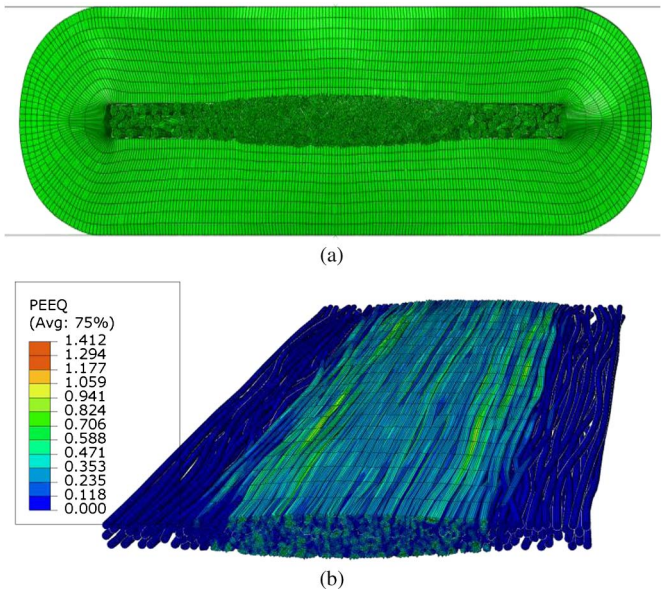

Fig. 7. After press operation. (a) Model cross section. (b) Filaments' equivalent plastic strain distribution for the case with press amount of 61%.

The definition of the contact area among filaments is shown in Fig. 5 (see the red region). Fig. 6 shows the model cross section after press operation and equivalent plastic strain distribution of filaments of 49.5%, and Figs. 7 and 8 show that of 61% and 70.5%, respectively. For the cases with press amounts of 49.5% and 54%, their cross sections show that there are large voids in the joint, the filaments do not contact well,

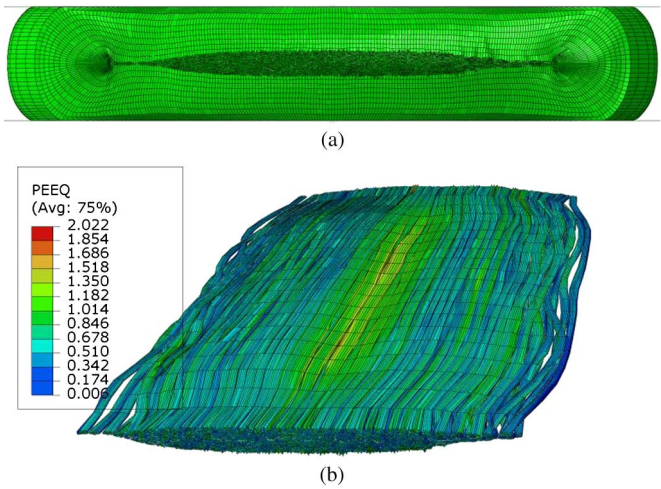

Fig. 8. After press operation. (a) Model cross section. (b) Filaments' equivalent plastic strain distribution for the case with press amount of 70.5%.

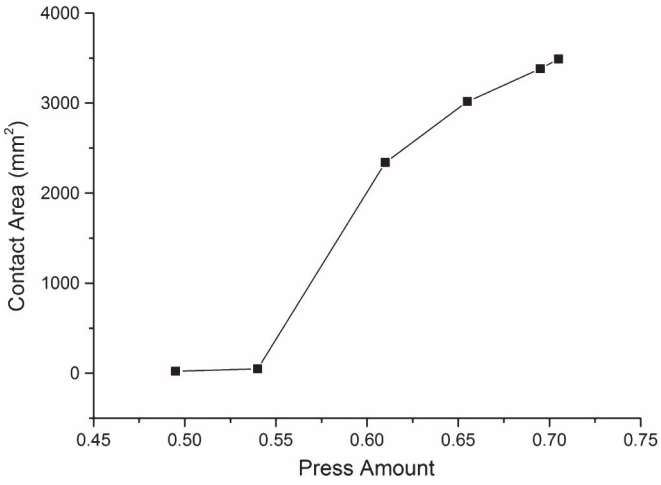

Fig. 9. Contact area of six models after press operation.

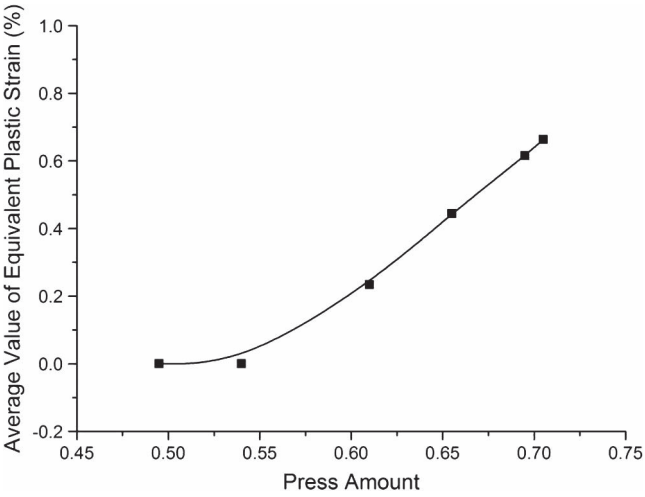

Fig. 10. Average value of equivalent plastic strain of six models' filaments after press operation.

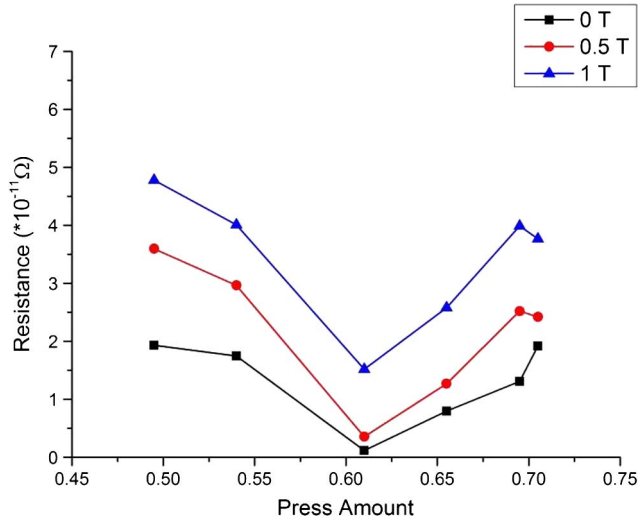

Fig. 11. Resistances of six samples in a 0–1-T background magnetic field.

and equivalent plastic strain distribution shows that very few filaments' equivalent plastic strain exceeds 11% to damage. For 61% and 65.5%, the cross section shows that there are few voids in the joint, the filaments contact well, and equivalent plastic strain distribution shows that strain is concentrated in the middle section relative to the edges; the equivalent plastic strain of filaments on the edges is less than 11%. For 69.5% and 70.5%, the cross section shows that there are no voids in the joint and the filaments contact very well, but equivalent plastic strain distribution shows that almost all the equivalent plastic strain of the superconducting filaments severely exceeds 11% to damage or even fracture. According to our assumptions aforementioned, we qualitatively consider the press amount 61%–65.5% to be the optimum range, in which the lowest joint resistance can be obtained.

Fig. 9 shows the contact area of six models after press operation. Fig. 10 shows the average value of equivalent plastic strain of the six models' filaments after press operation. In Figs. 9 and 10, we can see that as press amount increases, the contact area and average equivalent plastic strain will both increase. However, their increasing trends are different. The contact area slowly increases at first; then, after 54%, it increases very fast, but after 61%, it begins to slowly increase again to reach a stable value. Whereas, the average equivalent plastic strain slowly increases at first similarly, but after 54%, it can be considered to increase in an approximately linear form. The value of contact area and equivalent plastic strain can be used in further research based on the following equation:

$$R = f(S, \varepsilon^{\mathrm{pl}}) \tag{2}$$

where R is the joint resistance, and S and $\varepsilon^{\mathrm{pl}}$ are the contact area and equivalent plastic strain, respectively. The equation can be used to calculate the theoretical joint resistance value quantitatively, and we are still working on this.

IV. Experiment

Resistances of the six samples in a 0–1-T background magnetic field were tested using the current decay method to verify the conclusion we got from the simulation. Fig. 11 shows the results. We also used a scanning electron microscope (SEM) to observe cross sections of these samples, as shown in Fig. 12.

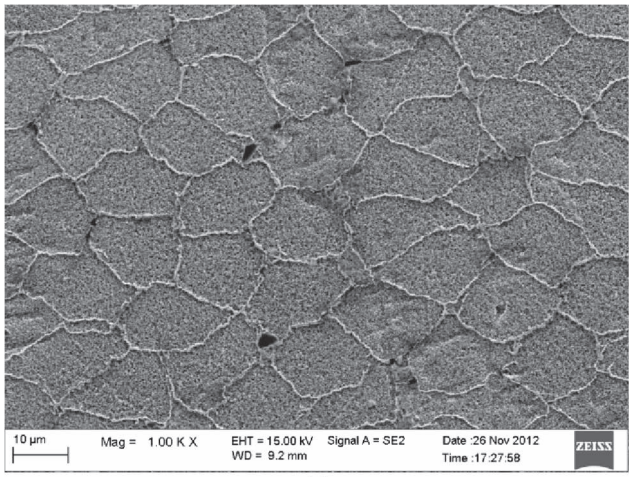

(a)

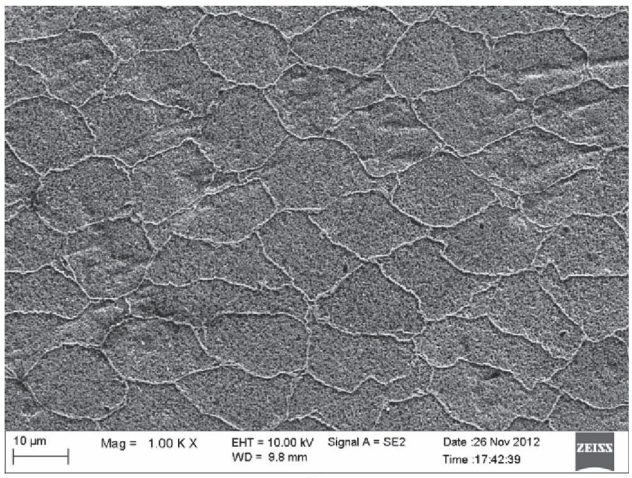

(b)

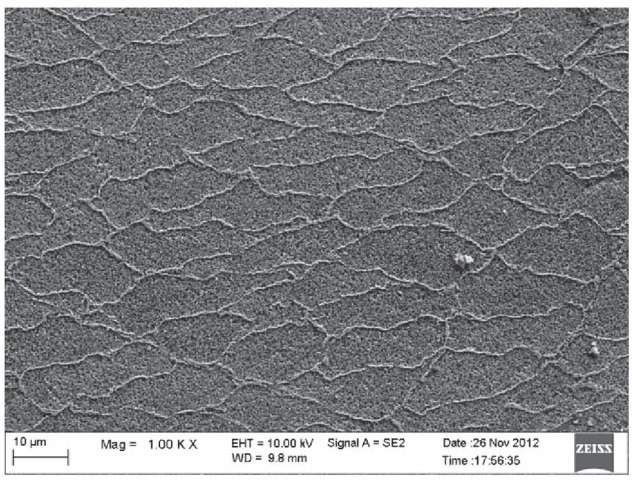

(c)

Fig. 12. Cross sections of joints with different press amounts: (a) 49.5%; (b) 61%; and (c) 70.5%.

Fig. 11 shows that the joint resistance increases with increasing background magnetic field; the joint resistances of 61% and 65.5% are smaller than the other samples, which correspond with the conclusion from the simulation.

Fig. 12(a) shows the cross section of the filaments after 49.5% press amount; there are some obvious voids, the filaments do not contact well, and the deformation of filaments is small. Fig. 12(b) shows the cross section of the filaments after 61% press amount; there are no obvious voids, the filaments contact well, and the deformation of filaments is moderate. Fig. 12(c) shows the cross section of the filaments after 70.5% press amount; there are no voids, the filaments contact more tightly, and the deformation of filaments is severe. These experimental results are indicated in Figs. 6–8.

TABLE II
JOINT RESISTANCE'S RELATIONSHIP WITH CONTACT AREA AND STRAIN DAMAGE FROM THE EXPERIMENT

Samples	Joint Resistance	Contact	Deformation
49.5%-54%	Relatively high	Not good	Small
61%-65.5%	Relatively Low	Good	Moderate
69.5%-70.5%	Relatively high	Very good	Severe

As shown in Table II, the resistance testing results and cross sections under the SEM of six samples demonstrate that the joint resistance's relationship with contact area and strain damage is as we predict. Our assumption of considering contact area and equivalent plastic strain to determine the joint's resistance qualitatively is appropriate.

V. CONCLUSION

Six NbTi cold-pressing welding superconducting joints were made at different press amounts for NMR application. This paper has used Abaqus–Explicit to do a quasi-static analysis of the cold-pressing welding process for these joints. In the simulation, two factors, namely, contact area and equivalent plastic strain, were mainly considered to determine the joint's resistance qualitatively. The simulation showed that a press amount of 61%–65.5% should be the optimum range. To verify the conclusion from our simulation, the resistances of six samples in a 0–1-T background magnetic field were tested by the current decay method and the cross sections of these joints were observed by a SEM. The experimental results agree well with the simulation ones. Further research on equation $R = f(S, \varepsilon^{\mathrm{pl}})$ will be carried out to calculate the theoretical joint resistance quantitatively.

REFERENCES

[1] Q. Wang, "High field superconducting magnet: Science, technology and applications," *Progr. Phys.*, vol. 33, no. 1, pp. 1–23, Feb. 2013.
[2] C. A. Swenson and W. D. Markiewicz, "Persistent joint development for high field NMR," *IEEE Trans. Appl. Supercond.*, vol. 9, no. 2, pp. 185–188, Jun. 1999.
[3] Q. Wang, *Practical Design of Magnetostatic Structure Using Numerical Methods*. Hoboken, NJ, USA: Wiley, Apr. 2013.
[4] P. Mclntyre, Y. Wu, G. Liang, and C. R. Meitzler, "Study of Nb_3Sn superconducting joints for very high magnetic field NMR spectrometers," *IEEE Trans. Appl. Supercond.*, vol. 5, no. 2, pp. 238–241, Jun. 1995.
[5] K. Seo, S. Nishijima, K. Katagiri, and T. Okada, "Evaluation of solders for superconducting magnetic shield," *IEEE Trans. Magn.*, vol. 27, no. 2, pp. 1877–1880, Mar. 1991.
[6] Q. Wang, X. Hu, S. Song, L. Ding, and L. Yan, "A method for the lower resistance superconducting joints with magnetic field shielded," Patent ZL201010123276.0, Sep. 14, 2011.
[7] J. Cheng, J. Liu, Z. Ni, C. Cui, S. Chen, S. Song, L. Li, Y. Dai, and Q. Wang, "Fabrication of NbTi superconducting joints for 400-MHz NMR application," *IEEE Trans. Appl. Supercond.*, vol. 22, no. 2, p. 4300205, Apr. 2012.

[8] H. M. Wen, L. Z. Lin, and S. Han, "Joint resistance measurement using current-comparator for superconducting wires in high magnetic field," *IEEE Trans. Magn.*, vol. 28, no. 1, pp. 834–836, Jan. 1992.
[9] Q. Wang, X. Hu, J. Cheng, L. Yan, H. Wang, and C. Cui, "Electromagnetic forming for the superconducting joints," Patents Cn 201210278270.X, Aug. 7, 2012.
[10] Dassault, *Abaqus Analysis User's Manual, Abaqus 6.11*, Champs Elysees, France, 2011.
[11] Q.-W. Wei, J.-S. Hu, L. Dong, Z.-M. Yan, Y.-W. Zhu, and Y. Wang, "Electromagnetic-structural coupling analysis of the pulse superconducting magnet based on ANSYS," *Sci. Technol. Eng.*, no. 15, pp. 4395–4397, Aug. 2009, In Chinese.

Feng Zhou, biography not available at the time of publication.

Junsheng Cheng, biography not available at the time of publication.

Jianhua Liu, biography not available at the time of publication.

Yinming Dai, biography not available at the time of publication.

Qiuliang Wang (SM'08) received the B.S. degree from Hubei University, Wuhan, China, in 1986, the M.S. degree from the Chinese Academy of Sciences (CAS), Hefei, China, in 1991, and the Ph.D. degree from CAS, Beijing, China, in 1994.

In 1996, he was a Postdoctoral Researcher with Kyushu University, Fukuoka, Japan. He has since been employed in several world-distinguished institutions, including the Korean Electrotechnology Research Institute; Samsung Advanced Institute of Technology; Oxford Instruments in the U.K.; German Heavy Ion Accelerator Center; Laboratory for Nuclear Science, Massachusetts Institute of Technology, Cambridge, MA, USA; AMS in CERN; The University of Queensland, Brisbane, Australia; and the University of Wollongong, Wollongong, Australia. Currently, he is a Professor and the Head of the Division of Superconducting Magnet Science and Technology, Institute of Electrical Engineering, CAS. His current research interests include large-scale applications of superconductivity technology in the space detector (AMS) and medicine (MRI and MSS), high-field scientific instruments, cryogenic engineering, numerical software, electromagnetic field, and the technology of material fabrication.

Namin Xiao, biography not available at the time of publication.

Luguang Yan, biography not available at the time of publication.